Calibration and sensitivity analysis of a basic polarimeter for manmade satellite observations

Marco F. Pirozzoli, Lucy A. Zimmerman, Michael Korta, Adrian D. Scheppe, Michael K. Plummer, Francis K. Chun
U.S. Air Force Academy, DFP, 2354 Fairchild Drive, Suite 2A31, USAF Academy, Colorado 80840
David M. Strong
Strong EO Imaging, Inc., 11175 Rocki Ln, Colorado Springs, Colorado 80908

ABSTRACT

The Department of Physics at the United States Air Force Academy has a DFM Engineering f/8.2, 16-inch telescope outfitted with a 9-position filter wheel populated with broadband photometric filters (Johnson-Cousins B, V, R, and a blue-blocking exoplanet filter) and a 100 lines per millimeter diffraction grating. As part of their senior capstone project, physics cadets developed a simple, four-channel polarimeter by populating the open slots in the filter wheel with linear polarized filters oriented at 0°, 45°, 90°, and 135° relative to the vertical axis of the imaging camera. Size and weight restrictions on the back of the telescope prohibited the use of more elaborate polarimeters. We developed the process and procedures to characterize the effect of the telescope optical elements on the polarization of incident light. Using an unpolarized, uniform flat light source, along with a polarized film rotated at 10° increments from 0° to 180°, the intensity of the light source was measured as it passed through the entire optical system including the as before mentioned linear polarized filters. The measured intensities were fitted to Malus Law using a least squares method. From this fit, a modified Mueller matrix was created that describes how the telescope's optical elements, including the polarizing filters, alter the incident light measured by the telescope's camera. In order to relate the measured intensities of light to the Stokes parameters of the light reflected from a satellite, a calibration matrix was computed using a pseudoinverse of the modified Mueller matrix. The sensitivity of the pseudoinverse process was analyzed by perturbing input data and measuring the RMS error between the perturbed and ideal matrices. This process for employing the pseudoinverse introduced minimal error into the system as the RMS error for the calibration matrix was within an acceptable error range. The calibration matrix was applied to satellite observations taken during the Fall 2019 equinox period and resulted in observed satellite Stokes parameters.

1. INTRODUCTION

At the beginning of the space age, very few manmade objects orbited the earth, so distinguishing them from one another was relatively straightforward. Today, as more nations and commercial companies venture into space, there will be far more satellites, rocket bodies, and debris to track and de-conflict. Current projections point to an increasingly dense space environment such that tracking, identifying, and characterizing each object will become an ever more daunting task. Imagery of artificial space objects, especially those in Geosynchronous Orbit (GEO), is predominantly unresolved, due to the high slant range. These objects appear as point sources of light which creates difficulties in distinguishing them from one another. However, previous research has shown that unresolved optical satellite signatures contain important information that can be used to characterize and distinguish one satellite from another.

As astronomical instrumentation has improved, considerable progress has been made in satellite characterization through the use of photometry [1-5] and spectral measurements [6] to classify both space debris and satellites in GEO. Although obtaining spectra using slitless spectroscopy techniques has been demonstrated for characterizing unresolved satellites [7-8], other than its application to astronomical objects [9], unresolved satellite polarimetry has not been explored to the same extent in the literature. Reference [10] demonstrated the usefulness of the polarimetry technique using a polarizing beam splitter to determine the horizontal and vertical linear Stokes parameter for light reflected off satellites and used that parameter to identify and categorize the objects. Reference [11] developed a process for calibrating the entire optical system, from aperture to focal plane array, utilizing a set of calibration images. This method is similar to methods used for individual polarimeters [12] but expanded to the entire optical

system all at once. A non-linear, least squares regression algorithm (e.g., Levenberg-Marquardt) is used to generate a matrix describing the change in the light's polarization as it passes through the optical system. The pseudoinverse (e.g., Moore-Penrose) of the above matrix results in a calibration matrix which allows us to determine Stokes parameters describing the polarization of the incoming light [13]. This paper describes the simple polarimeter for our 16-inch telescope, the calibration procedure we developed and used, a sensitivity analysis of the calibration matrix, and an example of a GEO satellite's polarization signature.

2. POLARIZATION PRINCIPLES

To observe polarization signatures from satellites, it is necessary to relate measured intensities to Stokes parameters, which are a representation of the light's orientation before it enters the optical system. To mathematically define this relationship, we must generate a matrix that allows the incident Stokes parameters to be calculated directly from measured intensities.

Depending on the relative phases of the superimposed reflected EM waves, light can be linearly, circularly, or elliptically polarized, and it is possible to describe this polarization structure of the wave using Stokes parameters,

$$\begin{aligned} S_0 &= I_{0^\circ} + I_{90^\circ} \\ S_1 &= I_{0^\circ} - I_{90^\circ} \\ S_2 &= I_{45^\circ} - I_{135^\circ} \end{aligned} \qquad (1)$$

where I_{0°, I_{45°, I_{90°, and I_{135° represent the intensity of light polarized in the direction indicated by the sub-indices in degrees. S_0 is the total intensity of the light, S_1 is the preference for horizontal (90°) or vertical (0°) orientation, and S_2 is the preference for 45° or 135° orientation The fourth Stokes parameter S_3, is the preference for right-hand or left-hand circular polarization, but is not measured by our instrument. Additionally, S_3 is due to the transmission of light through a medium which is not a feature expected from solar radiation reflecting off a satellite. These three components are the inputs of the Stokes parameter (Eqn. 2), encoding the polarization information into one mathematical entity [14].

$$S = \begin{bmatrix} S_0 \\ S_1 \\ S_2 \end{bmatrix} \qquad (2)$$

The Stokes parameter fully describes the polarization of the incoming light, but once the light passes through an optical system, its polarization properties can change; as a result, the Stokes parameter will be modified as shown in Eqn. 3, where S_{in} is the Stokes parameter before the light enters the optical system and S_{out} is the Stokes parameter as the light exits the optical system [15].

$$S_{out} = \boldsymbol{M} S_{in} \qquad (3)$$

A satellite's linear polarization signature, S_{in}, is the parameter we are ultimately interested in determining, so we developed the following procedure to reach that goal. The Mueller matrix, $\boldsymbol{M}$, is usually a 4×4 matrix that represents how the optical components in a measuring device modify the polarization of incident light. The matrix operates on S_{in} to yield a new output Stokes parameter, S_{out} (Eqn. 3). However, since our basic instrument only captures information related to the first three Stokes parameters ($S_0, S_1,$ and S_2) by measuring intensities through four linear analyzer filters, we must develop a calibration matrix ($\boldsymbol{W}$) that converts these measured intensities to the incoming Stokes parameters (Eqn. 4).

$$S_{in} = \boldsymbol{W} \begin{bmatrix} I_{0^\circ} \\ I_{45^\circ} \\ I_{90^\circ} \\ I_{135^\circ} \end{bmatrix}. \qquad (4)$$

To generate the $\boldsymbol{W}$ matrix, the intensities measured in the next section are fitted to Malus Law which describes the attenuation of light intensity or electromagnetic waves by a polarization filter.

$$I = I_{init} cos^2(\theta - \phi), \qquad (5)$$

where θ is the angle of the polarization film or generator (from 0° to 180°), ϕ is the angle of the analyzer filter (0°, 45°, 90° and 135°), and I_{init} is the initial light intensity. Using the expansion for cosine and a double angle identity, we can write Eqn. 5 as

$$I = \frac{a_n}{2}[1 + b_n \cos(2\theta)\cos(2\phi) + c_n \sin(2\theta)\sin(2\phi)], \qquad (6)$$

where a_n, b_n, and c_n are the measured Stokes component values for a given polarizing filter angle ϕ. In an ideal situation, the sinusoidal functions that contain ϕ as the argument [e.g., cos(2ϕ), sin(2ϕ)] are either 0 or ±1, corresponding to their respective ideal analyzer angle (0°, 45°, 90° and 135°). However, since we know that the actual analyzer angles of our simple polarimeter will be less than ideal, the cos(2ϕ) and sin(2ϕ) terms will be encapsulated into the b_n and c_n coefficients. Thus, the final equation used to fit the calibration intensity data to Malus Law is:

$$I = \frac{a_n}{2}[1 + b_n \cos(2\theta) + c_n \sin(2\theta)]. \qquad (7)$$

We can then generate the following 4×3 matrix $\boldsymbol{U}$:

$$\boldsymbol{U} = \begin{bmatrix} a_{0^\circ} & a_{0^\circ}b_{0^\circ} & a_{0^\circ}c_{0^\circ} \\ a_{45^\circ} & a_{45^\circ}b_{45^\circ} & a_{45^\circ}c_{45^\circ} \\ a_{90^\circ} & a_{90^\circ}b_{90^\circ} & a_{90^\circ}c_{90^\circ} \\ a_{135^\circ} & a_{135^\circ}b_{135^\circ} & a_{135^\circ}c_{135^\circ} \end{bmatrix} \qquad (8)$$

where each row represents the Mueller matrix components for a given analyzer angle ϕ. Because $\boldsymbol{U}$ is a rectangular matrix, we cannot simply determine its inverse in a straightforward manner. Instead, we apply a pseudoinverse method such as Moore-Penrose [15], on the $\boldsymbol{U}$ matrix to find the $\boldsymbol{W}$ calibration matrix:

$$\boldsymbol{W} = (\boldsymbol{U}^T * \boldsymbol{U})^{-1} * \boldsymbol{U}^{\boldsymbol{T}}. \qquad (9)$$

From this calibration matrix, the input Stokes parameters can be determined in terms of the measured intensities as shown by Equation 4. This way, $\boldsymbol{W}$ provides an analytical measure to determine errors in the calibration process by comparing a perturbed to an unperturbed $\boldsymbol{W}$ matrix and calculating the error propagation.

The calibration method outlined in this section provides a means to determine the Stokes parameters of incident light entering the optical system based on the light intensities measured by our simple polarimeter. It also provides a method to compare different polarization signatures using Stokes parameters. Finally, the resulting $\boldsymbol{W}$ matrix provides a succinct metric for determining the error in the polarization measurements introduced by the optical elements within our telescope/camera system.

3. INSTRUMENTATION AND PROCESSING

All data for this project were taken using a 16-inch f/8.2 Ritchey-Chrétien telescope from DFM Engineering located at the USAFA Observatory (Fig. 1). The telescope was fitted with an Andor Alta U47 1024×1024 pixel CCD camera, and four round polarization filters or analyzers were installed in the camera's filter wheel. These four filters are linear polarizers positioned so their axes aligned as close to the ideal analyzer angles of 0°, 45°, 90°, and 135° relative to the vertical axis of the camera's focal plane. The telescope and camera system was calibrated using a simple generator, consisting of an Alnitak Flatman unpolarized, uniform light source, and a linear polarizing film. The linear polarization film was mounted to the light source in a manner that allowed the film to freely rotate in front of the light source. As illustrated in Fig. 2, the plywood blocked out light from the edges of the light source, and the ring freely rotated with markings made every 10°. The ring had mounting screws so the film would be held in place and allowed to rotate.

Fig. 1. DFM Engineering 16-inch Telescope at USAFA.

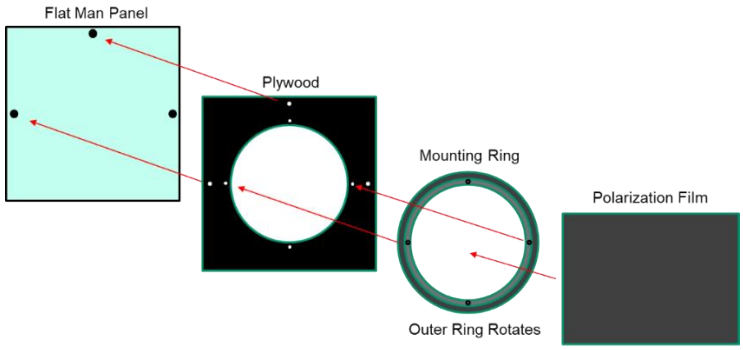

Fig. 2. Calibration device generator.

For each of the four analyzers in the filter wheel, 10 images with 5-second exposure times were taken at every 10° increment of the polarizing generator film between 0° and 180°. This resulted in 40 images per incremental film rotation yielding a total of 760 images, or 190 images per polarization filter. Fig. 3 below includes examples of the four filter images taken with the polarizing film positioned at 0°. The results are as expected: the 0° filter measures the highest average pixel count (3.92×10^4), whereas the 90° filter measures the lowest average pixel count (1.81×10^3). As predicted, the 45° and 135° filters measured roughly equivalent average pixel counts (2.14×10^4 and 1.85×10^4 respectively) approximately halfway between those seen in the 0° and 90° filters. To account for the camera's thermal noise level in the flat images, 10 dark images were taken with closed camera shutters and the same 5-second exposure time as the flat images.

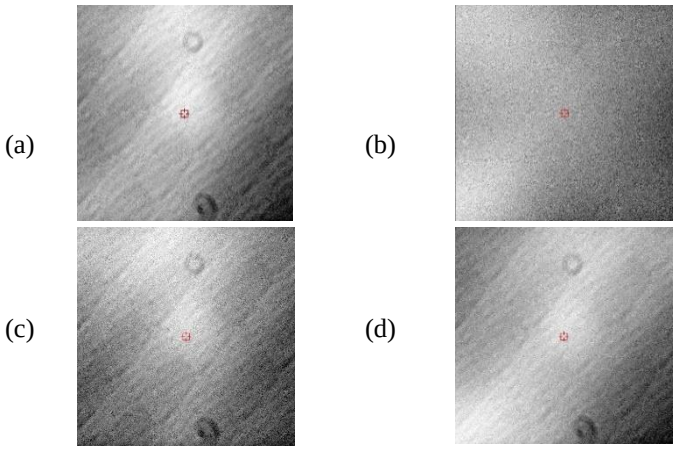

Fig. 3. Example flat images of the four filters (analyzers) when the polarizing film (generator) is at 0°: (a) represents the 0° filter, (b) represents the 90° filter, (c) represents the 135° filter, and (d) represents the 45° filter. The circular features are dust particles on the camera. As expected, the average recorded counts for the 90° filter are at a minimum when the counts for the 0° filter are at a maximum, while the 45° and 135° filters are approximately equal and half the value of the 0° filter.

The 10 flat and dark images for each filter angle and polarization film angle were separately stacked to calculate the average value of total counts for that specific subset of images. The resulting stacked dark images were subtracted from the stacked flat image of each filter to reduce the thermal noise in the flats. The average S_0 across the 19 angles for each of the corresponding filter pairs (i.e. 0° and 90°; 45° and 135°) was calculated:

$$S_{0:0^\circ+90^\circ} = \frac{\sum I_{0^\circ}+I_{90^\circ}}{19}, \qquad (10)$$

$$S_{0:45^\circ+135^\circ} = \frac{\sum I_{45^\circ}+I_{135^\circ}}{19}. \qquad (11)$$

The average count for each subset of images was divided by the corresponding S_0 value to get a normalized value of counts. The resulting calibration data can be seen in Fig. 4, which visually follows Malus Law.

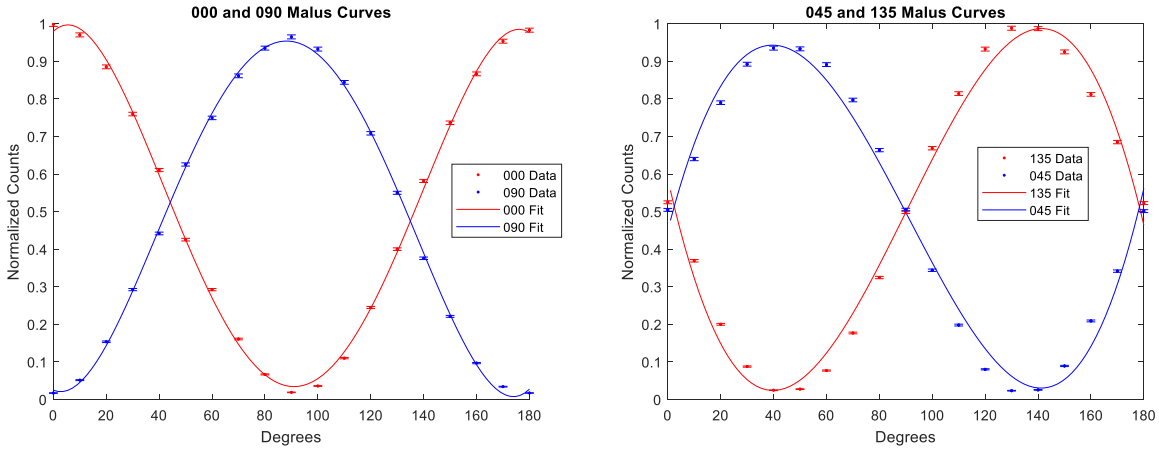

Fig. 4. The corresponding Malus curves for 0° and 90° (left panel) and 45° and 135° (right panel) with associated observed data points and error bars calculated using Poisson Statistics.

The measured data were input into the calibration process described in the previous section. The output coefficients of the Levenberg-Marquardt fit for each analyzer filter formed the elements of the $\boldsymbol{U}$ matrix

$$\boldsymbol{U} = \begin{bmatrix} 0.5063 & 0.4845 & 0.0195 \\ 0.4931 & -0.0008 & 0.4622 \\ 0.4922 & -0.4746 & 0.0323 \\ 0.5073 & 0.0116 & -0.4876 \end{bmatrix} \qquad (12)$$

which itself was inverted using the Moore-Penrose pseudoinverse to generate the $\boldsymbol{W}$ matrix:

$$\boldsymbol{W} = \begin{bmatrix} 0.4885 & 0.4870 & 0.5105 & 0.5150 \\ 1.0363 & 0.0063 & -1.0495 & -0.0222 \\ 0.0635 & 1.0140 & 0.0367 & -1.0846 \end{bmatrix}. \qquad (13)$$

The columns (left to right) in the $\boldsymbol{W}$ matrix represents the telescope-camera system's effects for the 0°, 45°, 90°, and 135° filters, respectively. The rows (top to bottom) represents the system's effects in the Stokes parameters S_0, S_1, and S_2, respectively. The $\boldsymbol{W}$ matrix given allows us to determine a satellite's Stokes parameter values (S_0, S_1, S_2), incident on the optical system, directly from its measured intensities using Equation 4. This matrix can also be compared to matrices with known perturbations to more completely understand the error introduced and propagated through the calibration process.

To provide a degree of confidence in our calibration approach, w calculate the actual analyzer angles using the appropriate elements of the $\boldsymbol{U}$ matrix. Following the approach by *Tippets et al.* [11], the Stokes parameters can be used to solve for the spherical coordinates in the Poincaré sphere. The polarization angle in the S_1 and S_2 plane can be found from the relationship $2\phi = \tan^{-1}(S_2/S_1)$, where ϕ is the analyzer angle. Because we encapsulated the

sinusoidal terms of the analyzer angle into the b_n and c_n coefficients in Equation (7), we can use those coefficients to calculate the angles. Table 1 shows the actual analyzer angles for each of the four polarization filters calculated from their appropriate fit coefficients ($U_{i,2}$ and $U_{i,3}$ where 'i' represents the row). The fact that we are within a couple of degrees to the ideal analyzer angles gives us confidence that the calibration of our simple polarimeter is reasonable.

Table 1 – Analyzer Angle Calculation

Ideal Analyzer Angle	Analyzer Angle Calculated from $\boldsymbol{U}$ Matrix	Absolute Difference
0°	-0.049°	0.049°
45°	43.848°	1.152°
90°	89.322°	0.678°
135°	136.949°	1.949°

4. SENSITIVITY ANALYSIS OF THE PSEUDOINVERSE

Utilizing a Moore-Penrose pseudoinverse is necessary to invert the non-square $\boldsymbol{U}$ matrix relating measured intensities to Stokes parameters (Eqn. 4). A pseudoinverse as opposed to a traditional inverse, introduces error into the calculation of the $\boldsymbol{W}$ matrix. In order to quantify this error, the amplitude was held constant at a normalized value of 1 and the analyzer angles were perturbed over a range of values from -5° to +5° in 0.01° increments. A set of ideal measured intensities can be calculated for the perturbed matrix using Malus Law (Eqn. 5). The ideal Stokes parameters were then computed directly from the intensities simulated at the 0°, 45°, 90°, and 135° angles using Equation 1. To measure the error introduced by the pseudoinverse alone, we isolate the pseudoinverse from the rest of the calibration process by assuming a perfect fit of data, removing the fit coefficients a_n, b_n and c_n from the expansion of Malus Law (Eqn. 6), and introducing a new term δ, which represents the perturbation of the analyzer angle ϕ (0°, 45°, 90°, or 135°)

$$I_{\phi}(\theta,\phi) = \tfrac{1}{2}[1 + \cos(2\theta)\cos(2[\phi+\delta]) + \sin(2\theta)\sin(2[\phi+\delta])] \qquad (14)$$

When no perturbations in the analyzer angle or amplitude are introduced, $\delta = 0$, and the cosine and sine terms with $2[\phi+\delta]$ in the argument collapse into 1, 0 or -1. To simulate a rotating light source, θ in Eqn. 15 is varied from 0° to 180° in 0.1° increments and a set of intensity measurements for the system is generated. To demonstrate these calculations, we select an arbitrary light source polarization angle ($\theta = 22.5°$), and compute the corresponding intensities using Equation 14:

$$\begin{aligned} I_{0^\circ} &= 0.8536 \\ I_{45^\circ} &= 0.8536 \\ I_{90^\circ} &= 0.1464 \\ I_{135^\circ} &= 0.1464. \end{aligned} \qquad (15)$$

Using Equation 1, the ideal Stokes parameters can be directly calculated from these four intensity measurements. For the given scenario of $\theta = 22.5°$, the Stokes parameters are:

$$\begin{aligned} S_0 &= 1 \\ S_1 &= 0.707 \\ S_2 &= 0.707. \end{aligned} \qquad (16)$$

Considering the assumptions stated above, the modified Mueller matrix, $\boldsymbol{U}$, can then be calculated using the first term and each successive term that includes the analyzer angle, ϕ, in its argument as shown in Equation 18.

$$\boldsymbol{U_{Ideal}} = \begin{bmatrix} \frac{1}{2} & \frac{1}{2}\cos[2(0°)]\cos(2[0°+0°]) & \frac{1}{2}\sin[2(0°)]\sin(2[0°+0°]) \\ \frac{1}{2} & \frac{1}{2}\cos[2(45°)]\cos(2[45°+0°]) & \frac{1}{2}\sin[2(45°)]\sin(2[45°+0°]) \\ \frac{1}{2} & \frac{1}{2}\cos[2(90°)]\cos(2[90°+0°]) & \frac{1}{2}\sin[2(90°)]\sin(2[90°+0°]) \\ \frac{1}{2} & \frac{1}{2}\cos[2(135°)]\cos(2[135°+0°]) & \frac{1}{2}\sin[2(135°)]\sin(2[135°+0°]) \end{bmatrix} \qquad (17)$$

$$\boldsymbol{U_{Ideal}} = \begin{bmatrix} 0.5 & 0.5 & 0 \\ 0.5 & 0 & 0.5 \\ 0.5 & -0.5 & 0 \\ 0.5 & 0 & -0.5 \end{bmatrix} \quad (18)$$

Taking the pseudoinverse of $\boldsymbol{U_{Ideal}}$, we calculate a $\boldsymbol{W}$ of

$$\boldsymbol{W} = \begin{bmatrix} 0.5 & 0.5 & 0.5 & 0.5 \\ 1 & 0 & -1 & 0 \\ 0 & 1 & 0 & -1 \end{bmatrix} \quad (19)$$

Applying the $\boldsymbol{W}$ matrix to the generated set of intensities in Equation 15, as shown in Equation 20, the Stokes parameters can be calculated for the perturbed matrix

$$\begin{aligned} S_{0_{Perturbed}} &= 1 \\ S_{1_{Perturbed}} &= 0.707 \\ S_{2_{Perturbed}} &= 0.707. \end{aligned} \quad (20)$$

Thus when there is no angle perturbation added, the root mean square error between the ideal and perturbed Stokes parameters for all angles of θ is 0. However, now a $\delta = +1°$ perturbation is introduced to the analyzer angle of the 0° filter. Once again, Stokes parameters can be calculated at each θ from 0° to 180° in 0.1° increments, and for the case in which θ = 22.5°.

$$\begin{aligned} S_0 &= 1 \\ S_1 &= 0.7314 \\ S_2 &= 0.6820 \end{aligned} \quad (21)$$

The $\boldsymbol{U}$ matrix is computed using Equation 17 as previously, but with a non-zero δ.

$$\boldsymbol{U} = \begin{bmatrix} 0.5 & 0.4997 & 0.0174 \\ 0.5 & 0 & 0.5 \\ 0.5 & -0.5 & 0 \\ 0.5 & 0 & -0.5 \end{bmatrix} \quad (22)$$

It is important to note that in the above $\boldsymbol{U}$ matrix, only the channel in which the perturbation was introduced (0° analyzer angle or row 1) experiences a change in values. None of the other rows or analyzer angles are affected. Computing the pseudoinverse of $\boldsymbol{U}$, we find a $\boldsymbol{W}$ of

$$\boldsymbol{W} = \begin{bmatrix} 0.5001 & 0.4913 & 0.4998 & 0.5088 \\ 1 & -0.0171 & -1.006 & 0.0178 \\ 0.0087 & 0.9911 & 0.0087 & -1.0086 \end{bmatrix} \quad (23)$$

Note that this time, the introduced perturbation in the 0° analyzer angle affects matrix columns 2-4, both of which are not associated with filters in which error was introduced. Applying the $\boldsymbol{W}$ matrix to intensity data of Eqn. 15, the perturbed Stokes parameters can be calculated at each θ from 0° to 180° in 0.1° increments. Once again, for the case in which θ = 22.5°,

$$\begin{aligned} S_{0_{Perturbed}} &= 0.9942 \\ S_{1_{Perturbed}} &= 0.7197 \\ S_{2_{Perturbed}} &= 0.6819, \end{aligned} \quad (24)$$

The root mean square difference between these two sets of Stokes parameters for a 180° rotation of the light source is thus

$$S_{0_{Error}} = 0.0062$$
$$S_{1_{Error}} = 0.0123 \quad (25)$$
$$S_{2_{Error}} = 0.0001.$$

This process of introducing a perturbation to the system and measuring the error in the resulting Stokes parameters was completed over a range of -5° to +5° in 0.01° increments for each of the four analyzer angles (0°, 45°, 90°, and 135°). Fig. 5 depicts the root mean square error for each analyzer angle.

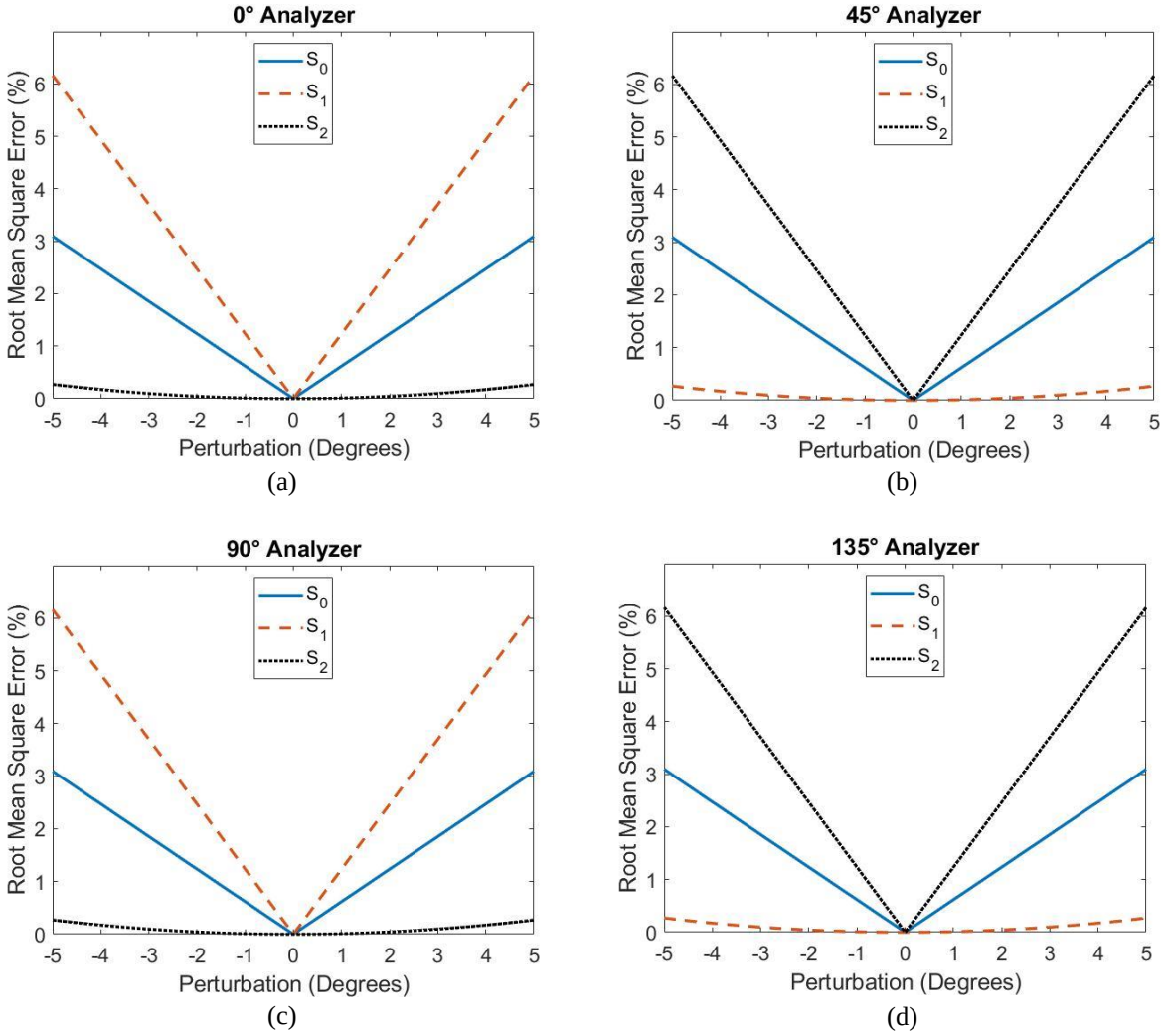

Fig. 5. Plot of Root Mean Squared error between the perturbed and ideal Stokes parameters for (a) the 0° polarization filter, (b) the 45° polarization filter, (c) the 90° polarization filter, and (d) the 135° polarization filter.

Over the examined interval, the root mean squared error introduced by the Moore-Penrose pseudoinverse for the S_0 Stokes parameter only slightly exceeds 3%. When a perturbation on an analyzer is introduced into the system, the Stokes parameter calculated using that analyzer has a more significant increase in error compared to the other two Stokes parameters. As expected, the Stokes parameter that does not use the perturbed analyzer in its calculation experiences minimal error. In other words, for the 0° and 90° analyzer plots (Figs. 5a-b), the angle perturbation has the greatest effect on S_1 (6%) and minor effect on S_2 (less than 0.5%) whereas the opposite is true for the 45° and 135° analyzer plots (Figs. 5c-d).

5. DEMONSTRATION

On 26 October 2019 (Universal Time), the 16-inch USAFA telescope with the polarimetry instrument attached, was used to observe DirecTV-15 (DTV-15), an operational communications satellite in GEO. The $\boldsymbol{W}$ matrix previously determined via the calibration process was applied to the satellite's intensity data measurements to generate a time series plot of Stokes parameters (Figs. 6 and 7) throughout the glinting phase, when the GEO satellite approaches a minimal solar phase angle, from approximately 0600 to 0700 UTC (26 October 2019). The data gap from approximately 0440 to 0510 is due to observing solar analog stars as a calibration source for satellite spectra collected at the same time as the satellite polarization measurements.

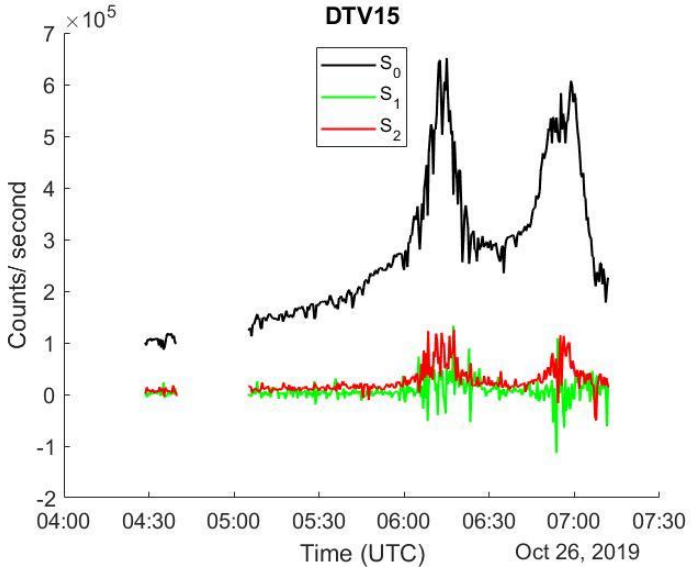

Fig. 6. Plots of S_0, S_1, and S_2 for DTV-15 observed on 26 Oct 2019 UTC. The satellite appears to glint twice. The data gap is associated with a time when the telescope was used to observe calibration stars. The figure displays counts per second of the incoming light on the vertical axis versus Universal Time on the horizontal axis. S_0 is represented by the black trace, while S_1 and S_2 are the green and red traces, respectively.

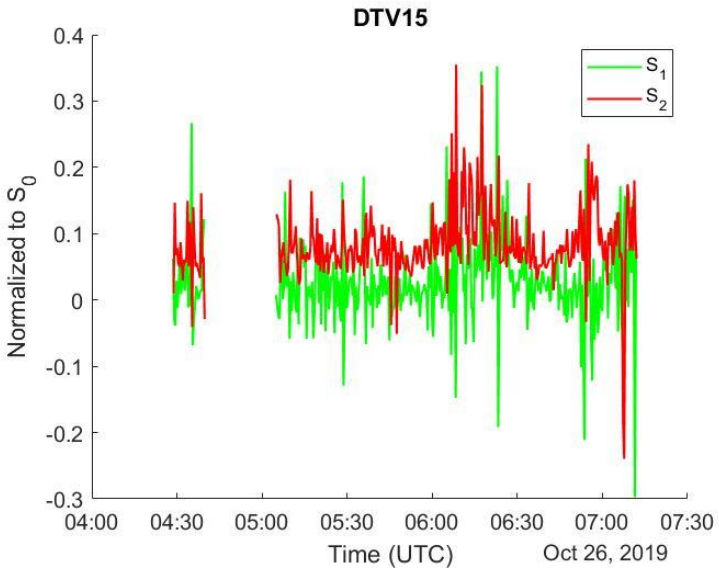

Fig. 7. Same data as Fig. 6, but with S_1 (green trace), and S_2 (red trace) normalized by S_0.

To first order, Fig. 6 shows that compared to the time period before it glints, DTV-15 exhibits greater variability in S_1 and S_2 Stokes parameters during both glint periods (0600-0630 UTC and 0645-0715 UTC). Fig. 7 presents the same data as Fig. 6 except with S_1 and S_2 normalized to S_0. During both glints, the S_1 and S_2 Stokes parameters trend positively, representing a polarization preference in the 0° and 45° direction. These plots of the Stokes parameters appear to show that the satellite's linear polarization is different during the glint compared to outside the glint period. More analysis of satellite polarization signatures with different buses and at different phase angles are clearly necessary, but this is a preliminary indication that polarization signatures can potentially be used to discern between resident space objects in GEO or even determine solar panel orientation with respect to a ground-based observer.

6. CONCLUSION

We have developed a basic polarization instrument for a DFM Engineering f/8.2, 16-inch telescope at the United States Air Force Academy in Colorado, and implemented a calibration process to characterize the effects of the telescope's optical components on any incident light. As a check on our calibration process, we calculated the actual analyzer angles of the polarization filters and found them to be within a couple of degrees of the ideal angles. We also determined that the use of the Moore-Penrose pseudoinverse to invert the Mueller matrix $\boldsymbol{U}$, introduced a small, but acceptable error into the telescope system's polarization calibration matrix $\boldsymbol{W}$. We have applied the $\boldsymbol{W}$ matrix generated by the calibration process to satellite data taken during glint season and shown that to first order, the satellite's polarization signature exhibits more variability during a glint compared non-glint times. Further analysis is clearly warranted, however we are confident that we have accurately calibrated USAFA's new four-channel polarimeter and are ready to use it for satellite optical characterization research.

7. ACKNOWLEDGEMENTS

The authors would like to acknowledge their colleague, Dr. Roger Tippets who was instrumental in this work, but who unfortunately passed away prior to presenting this work. We also want to acknowledge the support of the Air Force Office of Scientific Research. Additionally, this conference proceedings paper is the result of two senior capstone projects and two independent studies in the Department of Physics at the United States Air Force Academy. DISTRIBUTION STATEMENT A: Approved for public release: distribution unlimited. PA#: USAFA-DF-2020-306

8. REFERENCES

1. Payne, T. E., Gregory, S. A., Houtkooper, N. M., and Burdullis, T. W., "Classification of Geosynchronous Satellites Using Photometric Techniques," *Proceedings of the 2002 AMOS Technical Conference,* The Maui Economic Development Board, Inc., Kihei, Maui, HI (2002).
2. Payne, T. E., Gregory, S. A., and Luu, K., "SSA Analysis of GEOS Photometric Signature Classifications and Solar Panel Offsets," *Proceedings of the 2006 AMOS Technical Conference*, The Maui Economic Development Board, Inc., 667-673 (2006).
3. Vrba, F.J., DiVittorio, M.E., Hindsley, R.B., Schmitt, H.R., Armstrong, J.T., Shankland, P.D., Hutter, D.J., and Benson, J.A., "A survey of geosynchronous satellite glints." *The 2009 AMOS Technical Conference Proceedings*, The Maui Economic Development Board, Inc., Kihei, Maui, HI (2009).
4. Schildknecht, T., Musci, R., Flury, W., Kuusela J., de Leon, J., and de Fatima Dominguez Palmero, L., "Properties of High Area-to-Mass Ratio Space Debris Population in GEO," *The 2005 AMOS Technical Conference Proceedings*, The Maui Economic Development Board, Inc., Kihei, Maui, HI, 216-223 (2005).
5. Seitzer, P., Abercromby, K.J., Barker E.S., and Rodriguez H.M., "Optical Studies of Space Debris at GEO - Survey and Follow-up with Two Telescopes," *Proceedings of the 2007 AMOS Technical Conference*, The Maui Economic Development Board, Inc., Kihei, Maui, HI, 338-343 (2007).
6. Schildknecht, T., Vananti, A., Krag, H., and Erd, C., "Reflectance spectra of space debris in GEO," *The 2009 AMOS Technical Conference Proceedings*, The Maui Economic Development Board, Inc., Kihei, Maui, HI, 220-227 (2009).
7. Tippets, R.D., S. Wakefield, S. Young, I. Ferguson, C. Earp-Pitkins, and F.K. Chun, "Slitless spectroscopy of geosynchronous satellites," Opt. Eng. 54(10), 104103 (2015). doi: 10.1117/1.OE.54.10.104103.
8. Dunsmore, A.N., J.A. Key, R.M. Tucker, E.M. Weld, F.K. Chun, and R.D. Tippets, "Spectral Measurements of Geosynchronous Satellites During Glint Season," J. Spacecraft and Rockets, 7 October 2016. doi: http://arc.aiaa.org/doi/abs/10.2514/1.A33583.
9. W.A. Hiltner, "Polarization of Light From Distant Stars by Interstellar Medium", Science, 18 Feb 1949: Vol. 109, Issue 2825, pp. 165, DOI: 10.1126/science.109.2825.165
10. Speicher, Andy. "Identification of Geostationary Satellites Using Polarization Data from Unresolved Images", Ph.D. Thesis, University of Denver, (2015).
11. Tippets, Roger. "Polarimetric Imaging of Artificial Satellites", Ph.D. Thesis, The Union Institute and University, (2004).
12. Bailey, Jeremy et al. "A High-Sensitivity Polarimeter Using a Ferro-Electric Liquid Crystal Modulator." Monthly Notices of the Royal Astronomical Society 449.3 (2015): 3064–3073.
13. Penrose, R. "On Best Approximate Solutions of Linear Matrix Equations." Mathematical Proceedings of the Cambridge Philosophical Society, 52, Issue. 1, 17. (1956)
14. "Absorption Polarizers: Polaroid." Polarized Light, by Dennis H. Goldstein, Fourth ed., CRC Press, 503–509 (2011).
15. "Coherency Matrix and Stokes Vector." Polarized Light and the Mueller Matrix Approach, by Jose J. Gil Perez and Razvigor Ossikovski, CRC Press, 10-16 (2016).